iScience

CellPress
OPEN ACCESS

Article

S100A4/NF-κB axis mediates the anticancer effect of epigallocatechin-3-gallate in platinum-resistant ovarian cancer

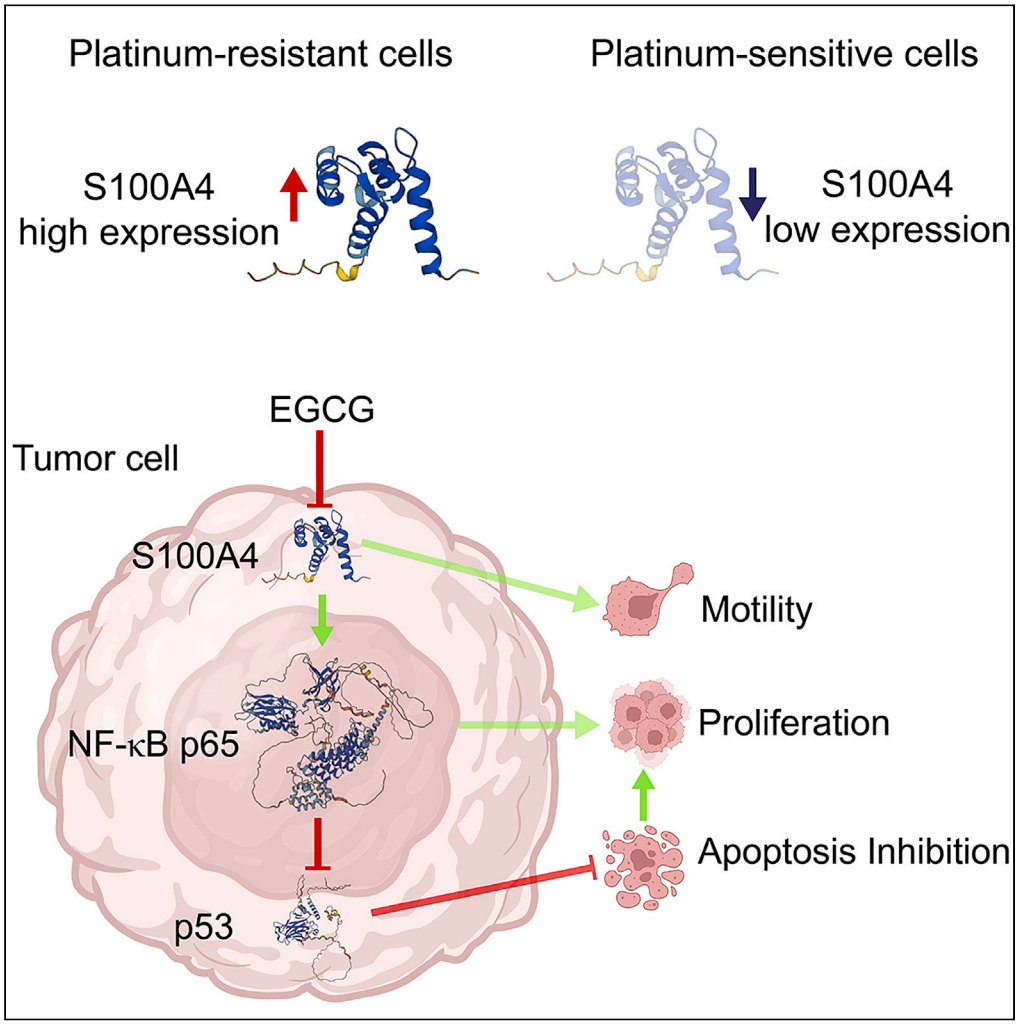

Xiaoli Li, Yidan Hou, Gaoyang Han, Yudan Yang, Shaofang Wang, Xiufang Lv, Ming Gao

gaoming330949@126.com

Highlights

EGCG inhibits proliferation, mobility, and induces apoptosis in OC/DDP cells

S100A4-inactivation decreases NF-κB expression while increasing p53 expression

EGCG-induced S100A4-inactivation slows tumor progression in OC/DDP xenograft mice

Li et al., iScience 27, 108885
February 16, 2024
https://doi.org/10.1016/j.isci.2024.108885

iScience

CellPress
OPEN ACCESS

Article

S100A4/NF-κB axis mediates the anticancer effect of epigallocatechin-3-gallate in platinum-resistant ovarian cancer

Xiaoli Li,[1,4] Yidan Hou,[1,4] Gaoyang Han,[2] Yudan Yang,[1] Shaofang Wang,[1] Xiufang Lv,[3] and Ming Gao[1,5,*]

SUMMARY

Resistance to cisplatin (*cis*-dichlorodiamineplatinum, DDP) in ovarian cancer is a significant clinical challenge. Epigallocatechin-3-gallate (EGCG) has shown promise in cancer therapy. However, its effects on DDP-resistant ovarian cancer remain understudied. This study aims to assess the impact of EGCG on DDP-resistant cells and elucidate the associated molecular mechanisms. DDP-resistant cell lines were utilized for biological characterization. EGCG effectively inhibited proliferation, mobility, and induced apoptosis in OC/DDP cells. It downregulated the expression of S100A4 and NF-κB while upregulating p53 expression. These effects were reversed upon overexpression of S100A4 or NF-κB. *In vivo* experiments confirmed tumor inhibition and KI67 inhibition by EGCG. Moreover, EGCG downregulated the expression of S100A4 and NF-κB while upregulating p53 in xenograft mice compared to those without EGCG treatment. This study suggests that EGCG suppresses cancer progression through the S100A4/NF-κB signaling pathway, involving interaction with p53. EGCG holds potential as an anticancer candidate for OC/DDP.

INTRODUCTION

Ovarian cancer (OC), recognized as a malignant disease, ranks first in lethality among women worldwide, constituting the seventh leading cause of tumor-associated morbidity and mortality.[1] The etiology underlying the incidence and poor prognosis of OC remains poorly understood.[2] Despite the emergence of various cancer therapies, platinum-based chemotherapy continues as the primary postoperative treatment for OC.[3] While the majority of OC cases initially respond to platinum-based doublet chemotherapy, 70%–85% of patients experience recurrence within three years, and approximately one-third exhibit poor response to platinum chemotherapy.[4] Despite the ongoing evolution of chemotherapy regimens, there has been no significant improvement in patient survival rates, largely due to chemotherapy resistance. Consequently, reversing drug resistance has become a focal point in OC treatment. The poor prognosis of platinum-resistant OC necessitates immediate adjustment of therapy to improve patient outcomes.

Green tea, containing the primary compound epigallocatechin-3-gallate (EGCG), has shown potential benefits in preventing and treating reproductive cancers, including ovarian, cervical, endometrial, and vulvar cancers.[5] The anticancer effects of EGCG may influence cancer processes, including initiation, progression, and metastasis.[6] S100A4, a member of the S100 protein family, consists of small Ca^{2+}-binding proteins with a molecular mass of 10–12 kDa.[7] S100 proteins participate in proliferation, differentiation, or apoptosis. The frequent upregulation of S100A4 in human malignancies contributes to oncogenic transformation, angiogenesis, mobility, and metastasis of tumor cells.[8,9] Although there is evidence suggesting that EGCG might impair the function of S100A4, further exploration of the exact molecular mechanism is necessary to draw definitive conclusions and formulate stronger recommendations for the potential use of green tea.

This study aims to investigate the relationship between the expression of S100A4 and EGCG in cisplatin (*cis*-dichlorodiamineplatinum, DDP)-resistant OC cell lines, providing a theoretical basis for clinical treatments to overcome drug resistance. Therefore, identifying factors related to chemotherapy sensitivity or resistance in OC is crucial to fundamentally increase drug efficacy, reduce toxicity and side effects, and guide clinical practice, representing a significant breakthrough in OC research.

RESULTS

DDP-resistant OC cells are resistant to DDP and sensitive to EGCG

Using CCK8, the cell viability of various DDP concentrations was assessed, and the IC50 for drug resistance was determined. SKOV3/DDP cells exhibited a DDP IC50 value of 89.83 μM, which was higher than that of SKOV cells (Figure 1A). Similarly, the IC50 of A2780/DDP cells was

[1]Department of Oncology, The First Affiliated Hospital of Zhengzhou University, Henan 450052, China
[2]Department of Thoracic Surgery, Zhengzhou Central Hospital, Henan 450052, China
[3]Department of Radiation Oncology, The First Affiliated Hospital of Zhengzhou University, Henan 450052, China
[4]These authors contributed equally
[5]Lead contact
*Correspondence: gaoming330949@126.com
https://doi.org/10.1016/j.isci.2024.108885

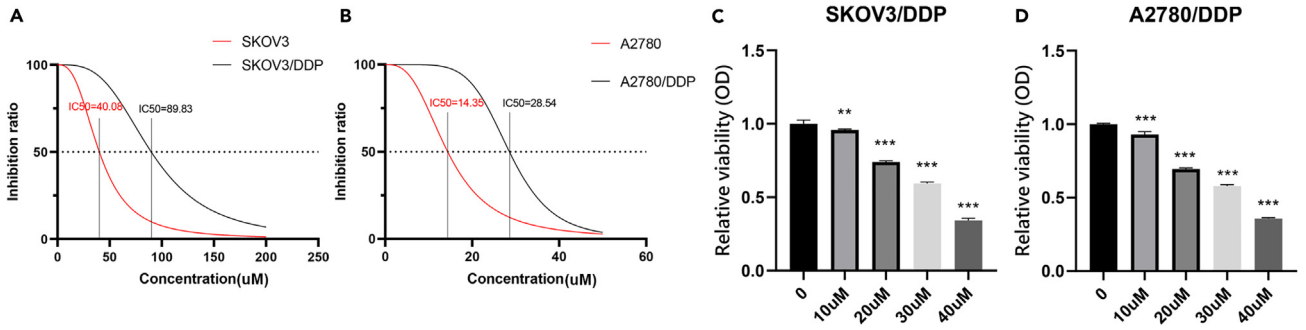

Figure 1. DDP-resistant and EGCG-sensitive cells verification

(A and B) The inhibition ratio of each OC cells in the presence of DDP detected by CCK-8.

(C and D) The relative viability of OC/DDP cells induced by different concentration of EGCG was analyzed by CCK-8.

Data were presented as mean ± SD, n = 3, differences among groups were assessed by ANOVA, **p < 0.01, ***p < 0.001.

28.54 μM, also higher than that of A2780 (Figure 1B). These findings indicate that these cells exhibit resistance to DDP. Subsequently, SKOV3/DDP and A2780/DDP cells were exposed to 0–40 μM EGCG, and the impact of the drug on DDP-resistant cells was evaluated (Figures 1C and 1D). EGCG exhibited a dose-dependent reduction in the viability of DDP-resistant cells, demonstrating that EGCG inhibits the growth of DDP-resistant cells. Ultimately, a concentration of 20 μM was selected for the functional study of DDP-resistant cells.

EGCG affected the proliferation, apoptosis, and mobility of DDP-resistant cells

In comparison to the blank group, the EGCG group displayed inhibitory effects on cells at various time points (Figure 2A). Colony formation assays with SKOV3/DDP and A2780/DDP cells yielded similar results ($p = 0.002$ and $p < 0.001$, Figure 2B). These findings indicate that EGCG treatment effectively inhibits the proliferation of SKOV3/DDP and A2780/DDP cells, with a stronger inhibitory effect observed in a time-dependent manner. The apoptotic rates of DDP-resistant cells treated with EGCG were evaluated through the TUNEL assay. As shown in Figure 2C, the apoptotic rates in the EGCG treatment groups increased to 2.3 and 2.1 times that of the blank group, respectively ($p = 0.008$, $p = 0.002$). Overall, these results demonstrate that EGCG can effectively inhibit cell growth and promote apoptosis in DDP-resistant OC cells.

A cell scratch assay was employed to assess the impact of EGCG on the migration capability of each group. The wound healing assay revealed a reduction in cell shedding and necrosis, along with slowed cell proliferation toward the midline. The scratch area healing rate was 23.055% ± 1.693% in the SKOV3/DDP EGCG treatment group and 21.204% ± 0.331% in the A2780/DDP EGCG treatment group, which was slower than that in the blank groups ($p < 0.001$, Figure 2D). The transwell method was employed to evaluate invasion ability, with results presented in Figure 2E. The relative invasion of SKOV3/DDP and A2780/DDP cells penetrating the membrane in the EGCG group was lower than that in the blank group ($p = 0.002$ and $p = 0.001$, respectively). These findings suggest that EGCG exerts an inhibitory effect on the migration and invasion capability of SKOV3/DDP and A2780/DDP cells.

Interactions between S100A4, NF-κB p65, and p53 in DDP-resistant OC cells

S100A4 exhibited upregulation in ovarian cancer tissues and cell lines when compared to normal tissues. Furthermore, the expression of S100A4 was increased in SKOV3/DDP and A2780/DDP cells compared to DDP-sensitive cells (Figures 3A–3C). To assess the influence of EGCG on downstream proteins' expression in SKOV3/DDP and A2780/DDP cells, EGCG was administered to treat DDP-resistant cells. Since nuclear factor κB (NF-κB) and p53 play roles in apoptosis, a feature altered in OC/DDP cells in the presence of EGCG, the impact of EGCG on NF-κB and p53 activity in the studied cell lines was examined. With NF-κB pathway activation, the p65 subunit is translocated into the nucleus. Thus, the presence of the p65 subunit was tested to assess NF-κB activity in SKOV3/DDP and A2780/DDP cells in the absence and presence of EGCG. The results indicated that EGCG treatment inhibited the expression of S100A4 and NF-κB p65 while promoting p53 expression (Figure 3D).

For further exploration, an S100A4 overexpression plasmid was constructed, and DDP-resistant cells were transfected to elucidate the impact of EGCG on cell functions and the mechanism underlying the changes in biological characteristics. Western blot analysis was employed to identify transfection efficiency, revealing that the plasmid transfected into cells restored S100A4 protein expression in EGCG-incubated cells (Figure 3E).

Overexpression of S100A4 rescinds the anticancer effect of EGCG on DDP-resistant OC cells

Verification of the effects of EGCG treatment and S100A4 overexpression on the proliferation of DDP-resistant cells was conducted through CCK8 identification and colony formation assays, as delineated in Figures 4A and 4B. The results indicated that EGCG treatment inhibited the proliferative effects of SKOV3/DDP and A2780/DDP cells. Conversely, the S100A4 overexpression with EGCG treatment in SKOV3/DDP and

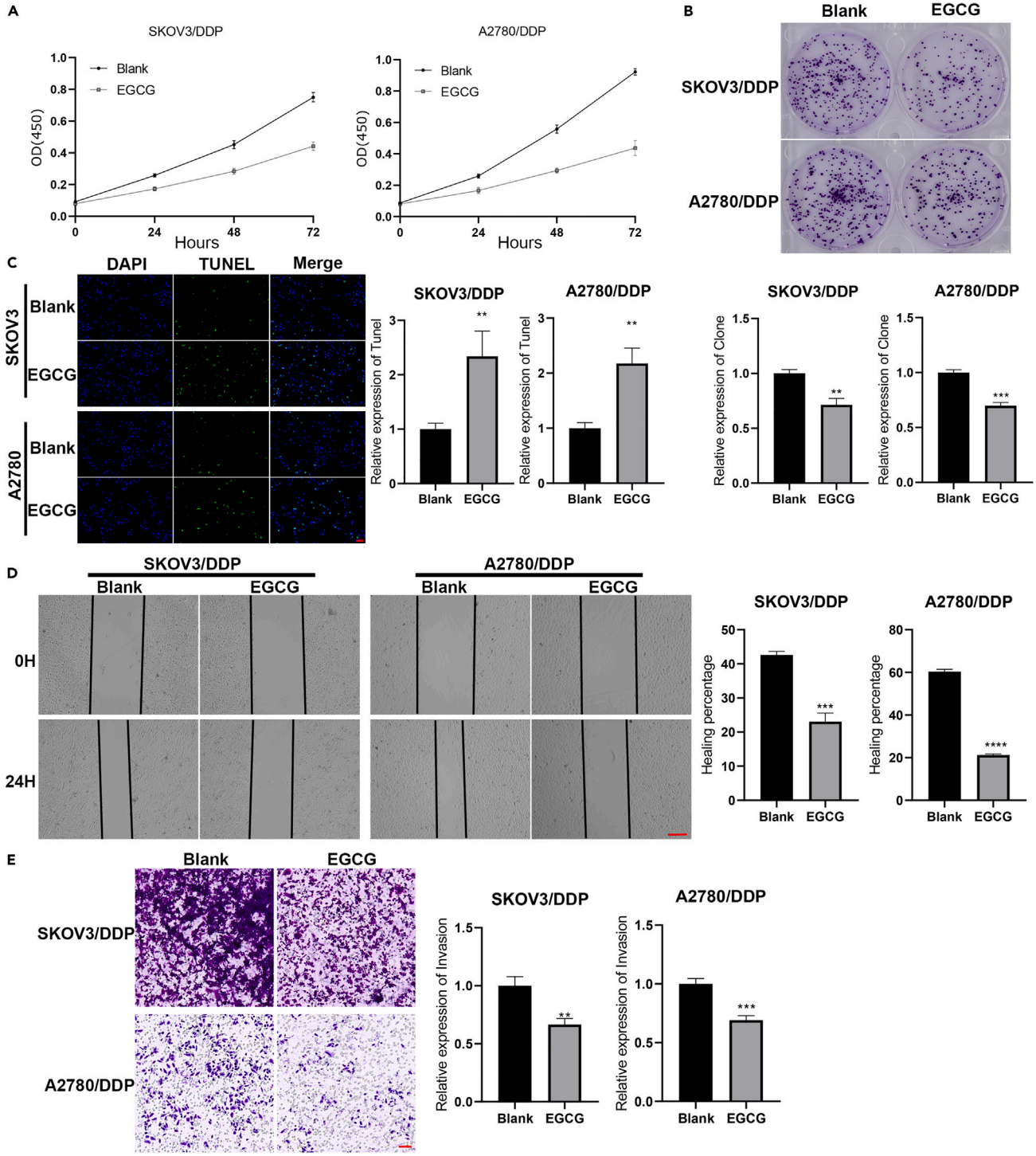

Figure 2. EGCG inhibits OC proliferation and malignancy profile

(A) SKOV3/DDP and A2780/DDP cells were incubated with indicated concentrations of EGCG for 24, 48, and 72 h, and CCK8 assay was performed to monitor cell viability.

(B) Cells were treated with EGCG for 48 h. Colonies formation assay were terminated after two weeks.

(C) Cell apoptosis was assessed by TUNEL test, scale bar, 50 μm.

(D) The migration of each group was detected by wound healing, scale bar, 500 μm.

(E) The number of cells that passed through Matrigel-coated membranes was accessed by Matrigel invasion assay, scale bar, 100 μm.

Graph data were presented as mean ± SD (n = 3), differences were assessed by Student's t tests, **p < 0.01, ***p < 0.001.

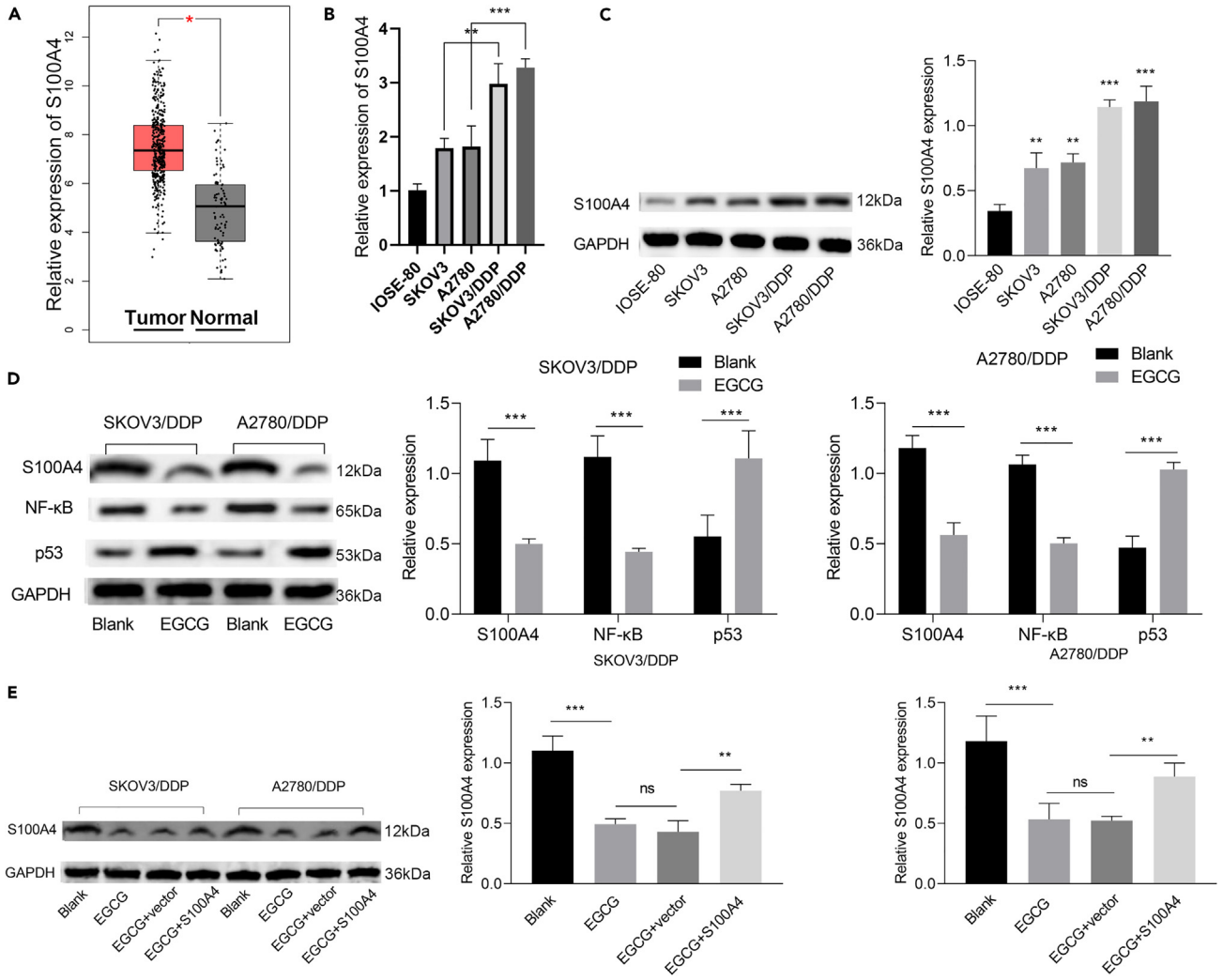

Figure 3. EGCG modulated S100A4, NF-κB p65, and p53 expression in DDP-resistant OC cells

(A) Bioinformatics prediction of S100A4 expression in OC, analyzed by GEPIA (including 426 tumor samples and 88 paired non-cancerous (normal) ovarian tissues).

(B and C) The mRNA and protein expression of S100A4 were detected by qRT-PCR and western blot in Human normal ovarian epithelial cells and OC cells.

(D) Western blot analysis showed the S100A4, NF-κB p65, and p53 expression with or without EGCG induced in DDP-resistant OC.

(E) Cells transfected with S100A4 plasmid restored the S100A4 expression which inhibited by EGCG, protein expression was analyzed by western blot.

Data were represented as mean ± SD, n = 3, differences among groups were assessed by ANOVA. **p < 0.01, ***p < 0.001, ns: no significantly.

A2780/DDP cells resulted in an opposite effect. Furthermore, S100A4 overexpression combined with EGCG reduced the apoptosis ratio, leading to opposite effects on apoptosis compared to EGCG treatment alone in SKOV3/DDP and A2780/DDP cells (Figures 4C and S1A). These results suggest that S100A4 indeed plays a pivotal role in OC/DDP cell growth and OC/DDP progression, which can be suppressed by EGCG.

Moreover, the invasion and metastasis abilities were attenuated in the EGCG incubation group, while mobility was enhanced in the S100A4 overexpression combined with EGCG group (Figures 4D, 4E, and S1B). Western blot analysis revealed that EGCG treatment and S100A4 overexpression reversed the inhibition of NF-κB p65 and the expression of p53 induced by EGCG treatment alone (Figure 4F). These findings indicate that EGCG modulates NF-κB and p53 expression via S100A4 to regulate proliferation and mobility.

NF-κB p65 overexpression induced proliferation, mobility, and apoptosis inhibition in S100A4-silenced DDP-resistant cells

The double luciferase experiment in HEK293T cells demonstrated that S100A4 can enhance the transcriptional activity of NF-κB p65 (Figure S2A). To further explore the comprehensive role of S100A4 in acquiring a tumor-promoting phenotype in SKOV3/DDP and A2780/DDP cells, si-S100A4 and NF-κB p65 plasmids were employed. Western blot analysis confirmed the silencing effect of si-S100A4 on

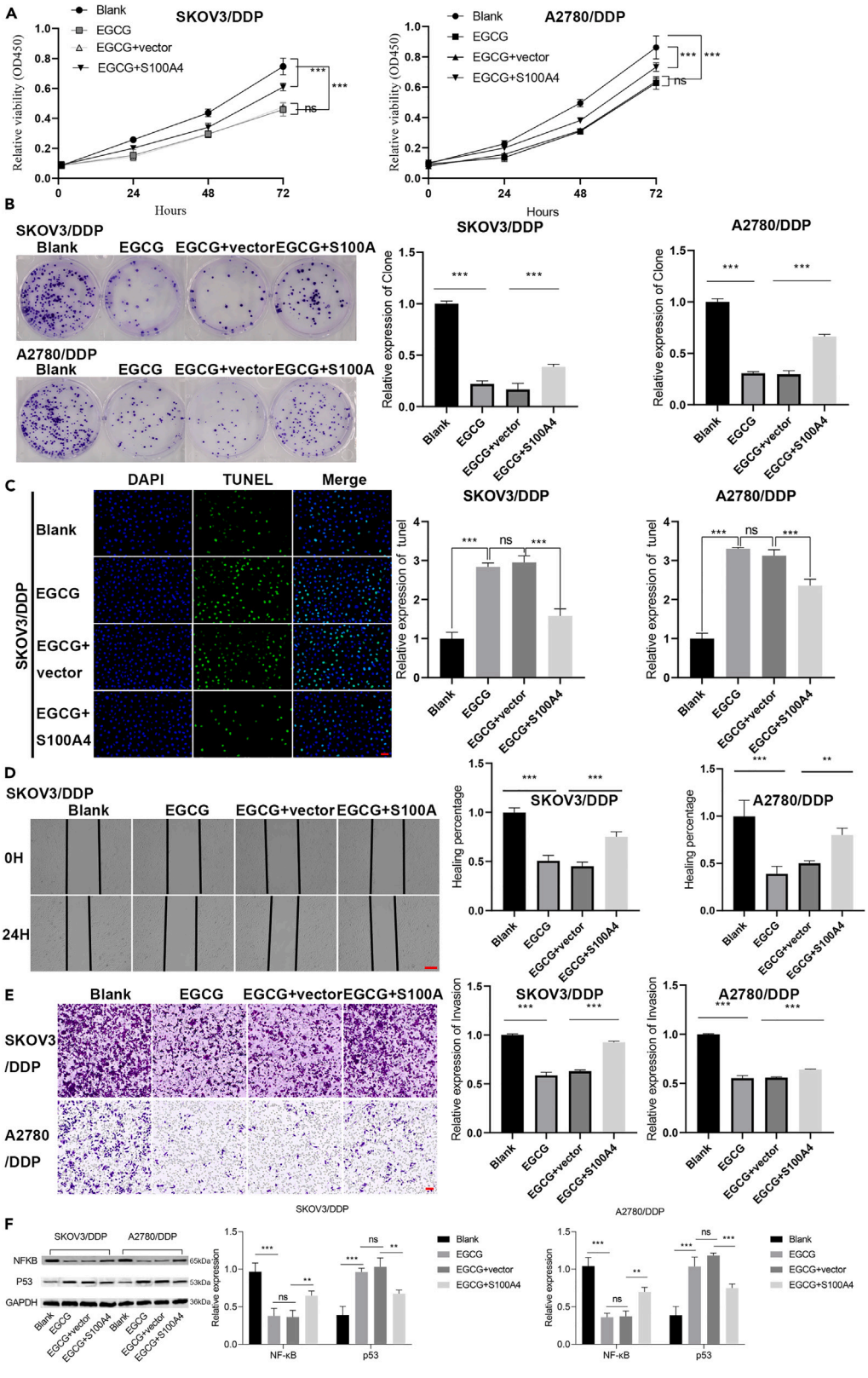
A
Blank
EGCG
EGCG+vector
EGCG+S100A4
SKOV3/DDP
A2780/DDP
Relative viability (OD450)
Hours
***
ns
B
SKOV3/DDP
A2780/DDP
Blank
EGCG
EGCG+vector
EGCG+S100A
Relative expression of Clone
C
DAPI
TUNEL
Merge
Blank
EGCG
EGCG+ vector
EGCG+ S100A4
Relative expression of tunel
D
0H
24H
Healing percentage
E
SKOV3 /DDP
A2780 /DDP
Relative expression of Invasion
F
NFKB
P53
GAPDH
65kDa
53kDa
36kDa
Relative expression
NF-κB
p53

Figure 4. S100A4 overexpression rescinds the anticancer effect of EGCG in DDP-resistant OC

(A) The cell viability of SKOV3/DDP and A2780/DDP cells were monitored by CCK8 assay for 24, 48, and 72 h. Four treatment groups included Blank, EGCG, EGCG + vector, and EGCG + S100A4.

(B) Cells transfected with S100A4 plasmid or vector plasmid were treated with EGCG for 48 h. Colonies formation assay were terminated after two weeks.

(C) Cell apoptosis was assessed by TUNEL test, scale bar, 50 μm.

(D) The migration of each group was detected by wound healing, scale bar, 500 μm.

(E) The number of cells that passed through Matrigel-coated membranes was accessed by Matrigel invasion assay, scale bar, 100 μm.

(F) NF-κB p65 and p53 expression were detected by western blot with vector or S100A4 overexpression.

ANOVA was used for differences among groups assessment, data were represented as mean ± SD (n = 3), **p < 0.01, ***p < 0.001, ns: no significantly.

S100A4 expression (Figure S2B). S100A4 knockdown led to a significant reduction in cell activity and colony formation, which was rescued by NF-κB p65 overexpression (Figures 5A and 5B). Additionally, cell apoptosis increased with S100A4 knockdown, but this effect was counteracted by NF-κB p65 overexpression (Figures 5C and S2C). The invasion and metastasis ability were weakened in the si-S100A4 group but enhanced by the expression of NF-κB p65 (Figures 5D, 5E, and S2D). These results suggest that S100A4 can increase the expression of NF-κB p65 to promote cell proliferation and enhance mobility. Western blot analysis confirmed that S100A4 knockdown resulted in a decrease in NF-κB p65 and an increase in p53; however, upregulation of NF-κB by transfection with NF-κB p65 inhibited the S100A4-induced increase in p53 (Figure 5F). This suggests that S100A4 promotes the expression of NF-κB, and NF-κB modulates the expression of p53 with an inhibitory effect.

EGCG suppressed tumor growth in A2780 cell xenograft mice

To investigate the function of EGCG on OC in a live animal model, we established mouse models with A2780 cell xenografts. In line with our *in vitro* findings, the treatment with EGCG resulted in a significant reduction in both tumor volume and weight, thereby signifying the inhibition of tumor growth *in vivo* (See Figures 6A and 6B). Immunohistochemical (IHC) analysis demonstrated a noteworthy suppression of S100A4 expression in the EGCG-treated group compared to the control group, indicating the inhibitory effect of EGCG on S100A4 expression (Figure 6C). Furthermore, the presence of KI67-positive staining, a nuclear antigen expressed in proliferating cells, exhibited a decline in the EGCG treatment group (Figure 6C). In comparison to the control group, the EGCG treatment group displayed a significant reduction in the expression of both S100A4 and NF-κB p65, while the expression of p53 increased (Figure 6D). In summary, it can be postulated that EGCG substantially hinders tumor growth and that S100A4 suppresses EGCG-induced p53 by elevating NF-κB levels *in vivo*.

DISCUSSION

In this study, a systematic exploration was conducted to investigate the function and molecular mechanisms of EGCG in the context of DDP-resistant OC. We demonstrated that EGCG suppressed proliferation and mobility through the S100A4/NF-κB axis, suggesting that EGCG is a potent agent in OC/DDP cells. EGCG, a polyphenol with therapeutic potential, is primarily derived from green tea and has been studied in cancer therapy.[10] However, few studies have investigated its role in DDP-resistant cancer. Platinum is a crucial chemotherapeutic agent for OC treatment. Nonetheless, platinum resistance poses a significant challenge in the clinic. The mechanisms of DDP resistance are complex, including decreased drug uptake, increased drug efflux, enhanced DNA damage repair, and alterations in apoptotic signaling pathways.[11] In this study, we confirmed that S100A4 was upregulated in DDP-resistant OC cells compared to DDP-sensitive cells, and DDP resistance in OC cells contributed to treatment failure and cancer progression. These results are consistent with a study showing that nuclear S100A4 expression was elevated in ovarian cancer and considered a prognostic biomarker for metachronous metastasis and overall survival of cancer patients.[12,13]

S100A4, also known as metastasin, belongs to the calcium-binding protein S100 family and is widely distributed in the nucleus, cytoplasm, and extracellular matrix. It serves crucial biological roles, encompassing angiogenesis, cell survival, migration, invasion, apoptosis, autophagy, and immune regulation.[14,15] Nuclear expression of S100A4 is implicated in the aggressive behavior of ovarian carcinoma.[16] EGCG has been recognized for its antioxidant, antiproliferative, antiangiogenic, and antimetastatic properties.[17–19] In our study, EGCG exhibited anticancer effects on DDP-resistant OC, including inhibiting proliferation, increasing apoptosis, and reducing mobility. These findings align with EGCG's role in various cancer therapies, such as bladder cancer, breast cancer, colorectal cancer, liver cancer, and lung cancer.[20–24] Nonetheless, further comprehensive evidence is necessary to elucidate the interaction between EGCG and S100A4. Our initial discovery revealed that OC/DDP cells cultured with EGCG displayed resistance to proliferation and inhibition of S100A4 expression. Conversely, S100A4 overexpression counteracted EGCG resistance and heightened the malignancy of OC/DDP cells. This enhancement included increased proliferation, reduced apoptosis, and enhanced migration, even in the presence of EGCG. These findings suggest that EGCG's anticancer mechanism operates through the S100A4 pathway.

NF-κB plays a pivotal role in immunity, inflammation, cell proliferation, survival, angiogenesis, and apoptosis.[25] Its influence on the initiation, progression, metastasis, and resistance of human cancers is substantial.[26,27] In our study, NF-κB induction increased cell proliferation and metastasis while reducing apoptosis, completely reversing the inhibitory effects of si-S100A4 on cell malignancy. Previous research has shown that S100A4 expression can inhibit IκBα degradation, leading to NF-κB activation.[28] However, there is limited research on the regulation of S100A4 expression, and the molecular mechanism behind S100A4 upregulation during chemotherapy warrants further investigation. Additionally, EGCG can inhibit the expression of certain transcription factors related to tumor development, such as Sp1, AP-1, and

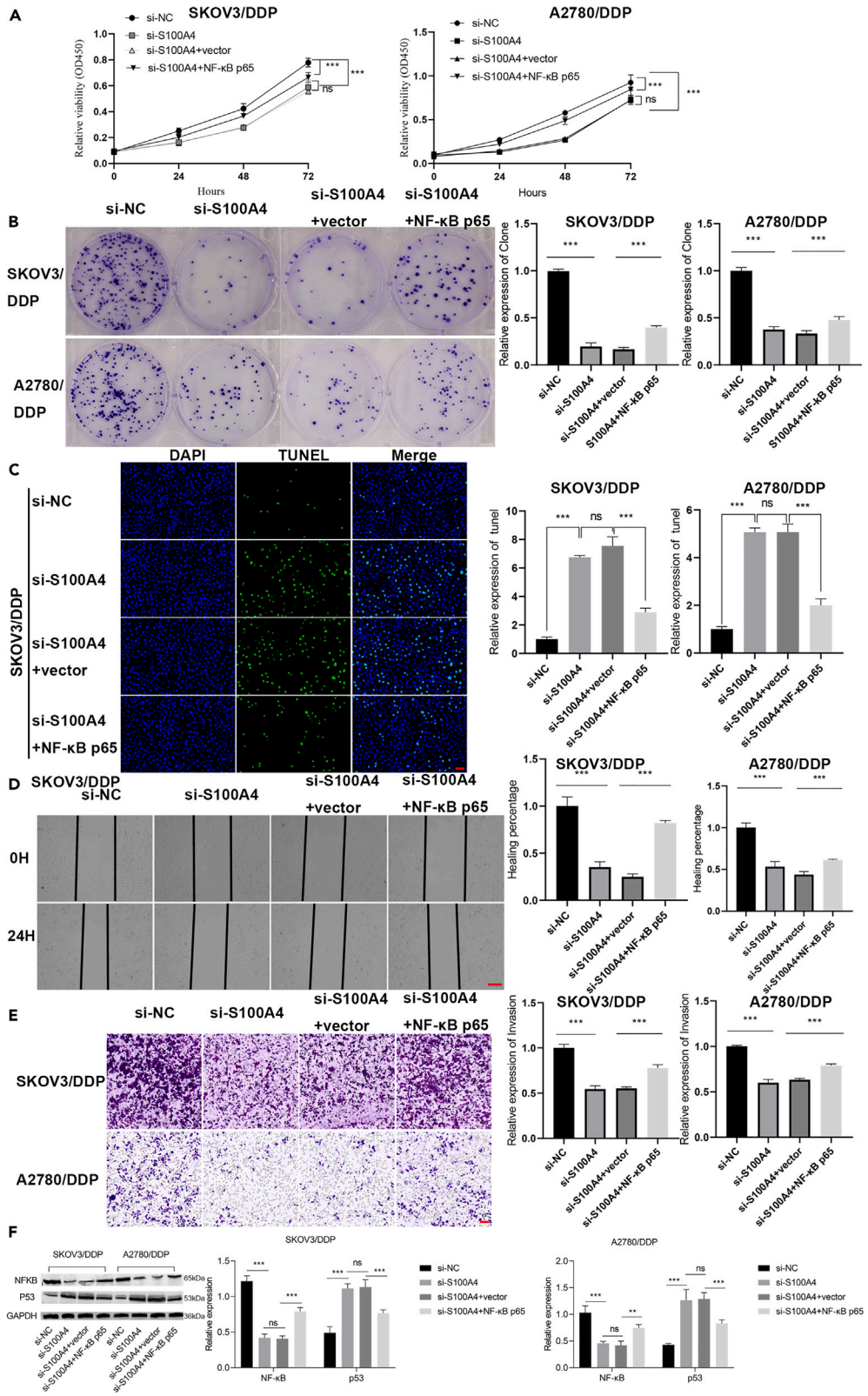
A
SKOV3/DDP
A2780/DDP
si-NC
si-S100A4
si-S100A4+vector
si-S100A4+NF-κB p65
Relative viability (OD450)
Hours
ns
***
B
SKOV3/
DDP
A2780/
DDP
si-NC
si-S100A4
si-S100A4
+vector
si-S100A4
+NF-κB p65
Relative expression of Clone
C
DAPI
TUNEL
Merge
SKOV3/DDP
Relative expression of tunel
D
0H
24H
Healing percentage
E
SKOV3/DDP
A2780/DDP
Relative expression of Invasion
F
NFKB
P53
GAPDH
65kDa
53kDa
36kDa
Relative expression
NF-κB
p53

Figure 5. NF-κB promotes OC progression in DDP-resistant cells

(A) The cell viability of SKOV3/DDP and A2780/DDP cells were monitored by CCK8 assay for 24, 48, and 72 h. Four treatment groups included si-NC, si-S100A4, si-S100A4 + vector, and si-S100A4 + NF-κB.

(B) Colonies formation assay was terminated after two weeks.

(C) Cell apoptosis was assessed by TUNEL test, scale bar, 50 μm.

(D) The migration of each group was detected by wound healing, scale bar, 500 μm.

(E) The number of cells that passed through Matrigel-coated membranes was accessed by Matrigel invasion assay, scale bar, 100 μm.

(F) NF-κB p65 and p53 expression were detected by western blot with vector or S100A4 overexpression.

ANOVA was used for differences among groups assessment, data were represented as mean ± SD (n = 3), **p < 0.01, ***p < 0.001, ns: no significantly.

NF-κB.[29,30] Numerous studies have demonstrated EGCG's ability to hinder NF-κB vitality or block UVB-induced NF-κB activation, thereby suppressing the NF-κB signaling pathway.[24,31,32] However, the specific mechanism of NF-κB inhibition remains unclear. These findings suggest that S100A4 and EGCG exert opposing effects on NF-κB, implying a potential relationship between EGCG and S100A4. To delve deeper into this connection, we transfected S100A4 overexpression, S100A4 silencing, and NF-κB overexpression into DDP-resistant OC cells. Our study revealed that NF-κB could disrupt S100A4 in HEK293T cells, and this interaction was further confirmed in SKOV3/DDP and A2780/DDP cells. Moreover, EGCG reduced the levels of both S100A4 and NF-κB, while S100A4 overexpression reversed the EGCG-induced reduction in NF-κB expression. This suggests that EGCG can directly bind to S100A4, blocking S100A4-induced NF-κB activation.

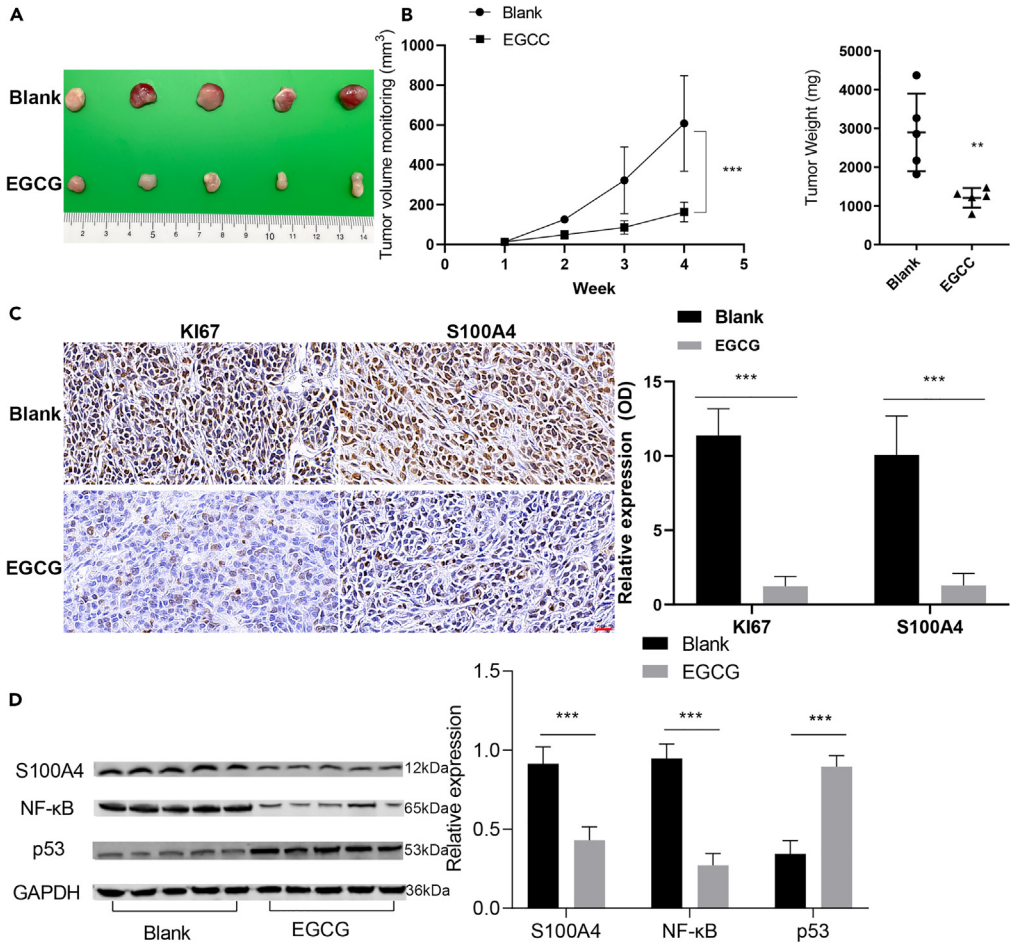

Figure 6. EGCG inhibited DDP resistance cells malignancy in xenografted A2780 cells

(A) Ten 5-week-old BALB/c nude mice were injected with 2 × 10^5 A2780 cells each. Two treatment groups included Blank and EGCG. Solid tumors were peeled from mouse subcutaneous tissue.

(B) Tumor size changed in a time-dependent manner, and tumor weight changes in two groups after sacrificed. In B of tumor volume, ANOVA was used for differences among groups assessment, in panel B of tumor weight, Student's *t* test was used.

(C) IHC staining of S100A4 and KI-67 in tumor tissues (40×), scale bar, 20 μm.

(D) Western blotting was used to assess S100A4, NF-κB p65, and p53 levels in tumor tissues, with GAPDH as an internal control.

In C and D, differences among groups were assessed by ANOVA, **p < 0.01, ***p < 0.001. Data are represented as mean ± SD (n = 5).

p53, functioning as a transcriptional regulator, induces apoptosis, promotes genomic stability, and inhibits angiogenesis.[33] A study demonstrated that members of the S100 family directly bind to p53, inhibiting its expression and phosphorylation, thereby contributing to chemoresistance and leading to cancer progression.[34] Although multiple studies have revealed a correlation between p53 function and OC, the modulation mechanism between S100A4 and p53 in OC requires further clarification.[35] Recent reports indicate that EGCG possesses anticancer activity, capable of inhibiting the PI3K/Akt and EGFR signal transduction pathways and upregulating p53 expression.[36–38] Nevertheless, the antitumor effects of EGCG in clinical contexts remain a subject of debate. In the current study, restoration of NF-κB through NF-κB p65 cDNA transfection in siS100A4 cells resulted in elevated proliferation and mobility, and inhibition of p53, elucidating that the inhibitory effect of NF-κB p65 on p53 and the S100A4/NF-κB axis represents the signaling pathway for EGCG's anticancer profile in OC/DDP cells.

To further verify the role of EGCG in inhibiting the proliferation of OC/DDP, an *in vivo* experiment was conducted, showing significant inhibition of tumor growth in mice treated with EGCG. The *in vivo* results revealed that EGCG treatment suppressed S100A4 expression and tumor growth via KI67. Additionally, EGCG treatment resulted in inhibition of the S100A4/NF-κB axis and upregulation of p53 in nude mice, suggesting that EGCG exerts anti-OC/DDP effects through the S100A4/NF-κB axis pathway.

Collectively, this study explored the molecular mechanisms and signaling pathways involved in EGCG-induced suppression of OC/DDP. Findings revealed the biological role for S100A4/NF-κB axis-related signaling in EGCG's anticancer function. Overexpression of S100A4, along with its interaction with NF-κB and p53, altered cell proliferation, apoptosis, and migration capabilities, each contributing to unfavorable outcomes in OC/DDP. EGCG emerges as a potential therapeutic agent to reverse DDP resistance and cancer progression through the S100A4/NF-κB axis.

Limitations of the study

We performed some bioinformatics analyses to study the S100A4 expression in ovarian cancer, but due to the information limitation of database, we could not know the expression of S100A4 between DDP resistance and DDP-sensitive samples. Future studies will involve collecting more clinical samples for more detailed analysis of S100A4, and even explore the NF-κB or p53 expression and the correlation of these proteins.

STAR★METHODS

Detailed methods are provided in the online version of this paper and include the following:

- KEY RESOURCES TABLE
- RESOURCE AVAILABILITY
  - Lead contact
  - Materials availability
  - Data and code availability
- EXPERIMENTAL MODEL AND STUDY PARTICIPANT DETAILS
  - Ethics approval and consent to participate
  - Cell lines
  - Mice
- METHOD DETAILS
  - Transfection
  - CCK8 testing
  - RNA extraction, reverse transcription and real-time quantitative PCR
  - Western blot analysis
  - Immunohistochemical (IHC) staining
  - TUNEL apoptosis assay
  - Transwell invasion test
  - Wound healing test
  - Colony formation
  - Double luciferase experiment
  - Nude mice tumorigenicity assay
- QUANTIFICATION AND STATISTICAL ANALYSIS

SUPPLEMENTAL INFORMATION

Supplemental information can be found online at https://doi.org/10.1016/j.isci.2024.108885.

ACKNOWLEDGMENTS

This work was supported by grants from the Henan Province Key Scientific Research Projects of Universities (grant number 21A320072), Medical Science and Technology Research Project of Henan Province (Joint construction project, grant number LHGJ20190014), and Henan Province Key Project of Medical Science and Technology Research Plan (grant number SBGJ202102138).

AUTHOR CONTRIBUTIONS

X. Li performed all experiments and wrote the manuscript. M.G. originally designed the research and supervised the study. X. Li, Y.H., Y.Y., and X. Lv performed the cell experiments. X. Li, G.H., Y.Y., and X. Lv performed the analysis. X. Li and G.H. drew the pictures. X. Li and S.W. generated the xenograft mice and performed the IHC assays. All the authors have read and approved the final manuscript.

DECLARATION OF INTERESTS

The authors declare no competing interests.

Received: September 18, 2023
Revised: December 6, 2023
Accepted: January 8, 2024
Published: January 12, 2024

REFERENCES

1. Siegel, R.L., Miller, K.D., and Jemal, A. (2020). Cancer statistics, 2020. CA. Cancer J. Clin. *70*, 7–30.
2. Momenimovahed, Z., Tiznobaik, A., Taheri, S., and Salehiniya, H. (2019). Ovarian cancer in the world: epidemiology and risk factors. Int. J. Women's Health *11*, 287–299.
3. Lheureux, S., Braunstein, M., and Oza, A.M. (2019). Epithelial ovarian cancer: evolution of management in the era of precision medicine. CA. Cancer J. Clin. *69*, 280–304.
4. Ledermann, J.A., Raja, F.A., Fotopoulou, C., Gonzalez Martin, A., Colombo, N., and Sessa, C.; ESMO Guidelines Working Group (2013). Newly diagnosed and relapsed epithelial ovarian carcinoma: ESMO clinical practice guidelines for diagnosis, treatment, and follow-up. Ann. Oncol. *24*, vi24–vi32.
5. Parish, M., Massoud, G., Hazimeh, D., Segars, J., and Islam, M.S. (2023). Green Tea in Reproductive Cancers: Could Treatment Be as Simple? Cancers *15*, 862.
6. Yang, H., Landis Piwowar, K., Chan, T.H., and Dou, Q.P. (2011). Green tea polyphenols as proteasome inhibitors: implication in chemoprevention. Curr. Cancer Drug Targets *11*, 296–306.
7. Dahlmann, M., Kobelt, D., Walther, W., Mudduluru, G., and Stein, U. (2016). S100A4 in Cancer metastasis: Wnt signaling-driven interventions for metastasis restriction. Cancers *8*, 59.
8. Donato, R., Cannon, B.R., Sorci, G., Riuzzi, F., Hsu, K., Weber, D.J., and Geczy, C.L. (2013). Functions of S100 proteins. Curr. Mol. Med. *13*, 24–57.
9. Helfman, D.M., Kim, E.J., Lukanidin, E., and Grigorian, M. (2005). The metastasis associated protein S100A4: role in tumour progression and metastasis. Br. J. Cancer *92*, 1955–1958.
10. Hasan, G.M., Hassan, M.I., Sohal, S.S., Shamsi, A., and Alam, M. (2023). Therapeutic targeting of regulated signaling pathways of non-small cell lung carcinoma. ACS Omega *8*, 26685–26698.
11. Galluzzi, L., Senovilla, L., Vitale, I., Michels, J., Martins, I., Kepp, O., Castedo, M., and Kroemer, G. (2012). Molecular mechanisms of cisplatin resistance. Oncogene *31*, 1869–1883.
12. Yan, W., Chen, J., Chen, Z., and Chen, H. (2016). Deregulated miR-296/S100A4 axis promotes tumor invasion by inducing epithelial-mesenchymal transition in human ovarian cancer. Am. J. Cancer Res. *6*, 260–269.
13. Maelandsmo, G.M., Flørenes, V.A., Nguyen, M.T.P., Flatmark, K., and Davidson, B. (2009). Different expression and clinical role of S100A4 in serous ovarian carcinoma at different anatomic sites. Tumour Biol. *30*, 15–25.
14. Ambartsumian, N., Klingelhöfer, J., and Grigorian, M. (2019). The Multifaceted S100A4 Protein in Cancer and Inflammation. Methods Mol. Biol. *1929*, 339–365.
15. Boye, K., and Maelandsmo, G.M. (2010). S100A4 and metastasis: a small actor playing many roles. Am. J. Pathol. *176*, 528–535.
16. Kikuchi, N., Horiuchi, A., Osada, R., Imai, T., Wang, C., Chen, X., and Konishi, I. (2006). Nuclear expression of S100A4 is associated with aggressive behavior of epithelial ovarian carcinoma: an important autocrine/paracrine factor in tumor progression. Cancer Sci. *97*, 1061–1069.
17. Cione, E., La Torre, C., Cannataro, R., Caroleo, M.C., Plastina, P., and Gallelli, L. (2019). Quercetin, Epigallocatechin Gallate, Curcumin, and Resveratrol: From Dietary Sources to Human MicroRNA Modulation. Molecules *25*, 63.
18. Ghasemi, F., Shafiee, M., Banikazemi, Z., Pourhanifeh, M.H., Khanbabaei, H., Shamshirian, A., Amiri Moghadam, S., Aref Nezhad, R., Sahebkar, A., Avan, A., and Mirzaei, H. (2019). Curcumin Inhibits NF-KB and Wnt/β-Catenin Pathways in Cervical Cancer Cells. Pathol. Res. Pract. *215*, 152556.
19. Liang, C., Yi, K., Zhou, X., Li, X., Zhong, C., Cao, H., Xie, C., and Zhu, J. (2023). Destruction of the Cellular Antioxidant Pool Contributes to Resveratrol-Induced Senescence and Apoptosis in Lung Cancer. Phytother Res. *37*, 2995–3008.
20. Piwowarczyk, L., Stawny, M., Mlynarczyk, D.T., Muszalska-Kolos, I., Goslinski, T., and Jelińska, A. (2020). Role of Curcumin and (-)-Epigallocatechin-3-O-Gallate in Bladder Cancer Treatment: A Review. Cancers *12*, 1801.
21. Romano, A., and Martel, F. (2021). The Role of EGCG in Breast Cancer Prevention and Therapy. Mini Rev. Med. Chem. *21*, 883–898.
22. Wu, W., Gou, H., Xiang, B., Geng, R., Dong, J., Yang, X., Chen, D., Dai, R., Chen, L., and Liu, J. (2022). EGCG Enhances the Chemosensitivity of Colorectal Cancer to Irinotecan through GRP78-MediatedEndoplasmic Reticulum Stress. J. Oncol. *2022*, 7099589.
23. Sojoodi, M., Wei, L., Erstad, D.J., Yamada, S., Fujii, T., Hirschfield, H., Kim, R.S., Lauwers, G.Y., Lanuti, M., Hoshida, Y., et al. (2020). Epigallocatechin Gallate Induces Hepatic Stellate Cell Senescence and Attenuates Development of Hepatocellular Carcinoma. Cancer Prev. Res. *13*, 497–508.
24. Alam, M., Ali, S., Ashraf, G.M., Bilgrami, A.L., Yadav, D.K., and Hassan, M.I. (2022). Epigallocatechin 3-gallate: From green tea to cancer therapeutics. Food Chem. *379*, 132135.
25. Xia, L., Tan, S., Zhou, Y., Lin, J., Wang, H., Oyang, L., Tian, Y., Liu, L., Su, M., Wang, H., et al. (2018). Role of the NF-κB-signaling pathway in cancer. OncoTargets Ther. *11*, 2063–2073.
26. Wu, K.J., Zhong, H.J., Yang, G., Wu, C., Huang, J.M., Li, G., Ma, D.L., and Leung, C.H. (2018). Small molecule Pin1 inhibitor blocking NF-κB signaling in prostate cancer cells. Chem. Asian J. *13*, 275–279.
27. Yang, G.J., Song, Y.Q., Wang, W., Han, Q.B., Ma, D.L., and Leung, C.H. (2021). An optimized BRD4 inhibitor effectively eliminates NF-κB-driven triple-negative breast cancer cells. Bioorg. Chem. *114*, 105158.
28. Boye, K., Grotterød, I., Aasheim, H.C., Hovig, E., and Maelandsmo, G.M. (2008). Activation of NF-κB by extracellular S100A4: Analysis of signal transduction mechanisms and identification of target genes. Int. J. Cancer *123*, 1301–1310.
29. Shimizu, M., Shirakami, Y., and Moriwaki, H. (2008). Targeting receptor tyrosine kinases for chemopreven-tion by green tea catechin, EGCG. Int. J. Mol. Sci. *9*, 1034–1049.
30. Shimizu, M., and Weinstein, I.B. (2005). Modulation of signal transduction by tea catechins and related phytochemicals. Mutat. Res. *591*, 147–160.
31. Aggarwal, B.B., and Shishodia, S. (2006). Molecular targets of dietary agents for prevention and therapy of cancer. Biochem. Pharmacol. *71*, 1397–1421.
32. Smith, D.M., Wang, Z., Kazi, A., Li, L.H., Chan, T.H., and Dou, Q.P. (2002). Synthetic analogs of green tea polyphenols as proteasome inhibitors. Mol. Med. *8*, 382–392.
33. Tanaka, T., Watanabe, M., and Yamashita, K. (2018). Potential therapeutic targets of TP53 gene in the context of its classically canonical functions and its latest non-canonical functions in human cancer. Oncotarget *9*, 16234–16247.

34. Duffy, M.J., Synnott, N.C., and Crown, J. (2017). Mutant p53 as a target for cancer treatment. Eur. J. Cancer *83*, 258–265.

35. Semczuk, A., Gogacz, M., Semczuk-Sikora, A., Jóźwik, M., and Rechberger, T. (2017). The putative role of TP53 alterations and p53 expression in borderline ovarian tumors-correlation with clinicopathological features and prognosis: a minireview. J. Cancer *8*, 2684–2691.

36. Liu, S., Wang, X.J., Liu, Y., and Cui, Y.F. (2013). PI3K/AKT/mTOR signaling is involved in (-)-epigallocatechin-3-gallate-induced apoptosis of human pancreatic carcinoma cells. Am. J. Chin. Med. *41*, 629–642.

37. Pan, M.H., Lin, C.C., Lin, J.K., and Chen, W.J. (2007). Tea polyphenol (-)-epigallocatechin 3-gallate suppresses heregulin-beta1-induced fatty acid synthase expression in human breast cancer cells by inhibiting phosphatidylinositol 3-kinase/Akt and mitogen-activated protein kinase cascade signaling. J. Agric. Food Chem. *55*, 5030–5037.

38. Hastak, K., Gupta, S., Ahmad, N., Agarwal, M.K., Agarwal, M.L., and Mukhtar, H. (2003). Role of p53 and NF-kappaB in epigallocatechin-3-gallate-induced apoptosis of LNCaP cells. Oncogene *22*, 4851–4859.

STAR★METHODS

KEY RESOURCES TABLE

REAGENT or RESOURCE	SOURCE	IDENTIFIER
Antibodies		
Rabbit anti-S100A4	Proteintech	Cat# 16105-1-AP; RRID:AB_11042591
Rabbit anti-NF-κB p65	Proteintech	Cat# 10745-1-AP; RRID:AB_2178878
Rabbit anti-p53	Proteintech	Cat# 60283-2-Ig; RRID:AB_2881401
Rabbit anti-GAPDH	DaiGe	db106
IRDye 680RD goat anti-rabbit	Licor	Cat# 925-68071; RRID:AB_2721181
Rabbit anti-S100A4	Servicebio	GB11397
Rabbit anti-KI67	Servicebio	Cat# GB111499; RRID:AB_2927572
HRP labeled goat anti rabbit IgG	Servicebio	Cat# GB23303; RRID:AB_2811189
Biological samples		
Mouse tissue specimens	This paper	N/A
Chemicals, peptides, and recombinant proteins		
Puromycin	Solarbio	P8230
RIPA buffer	JingCai	JC-PL001
Western Marker	Biosharp	BL712A
CCK-8	OuSe Biotech	C200-100
DAB	servicebio	G1212-200T
PMSF(100mM)	Solarbio	P0100
pancreatin	Servicebio	G4004
EDTA	iosharp	BL727B
Critical commercial assays		
CCK-8	OuSe Biotech	C200-100
TRIzol reagent	Invitrogen	15596026
2 x SYBR Green	Servicebio	G3321-15
RNA reverse transcription kit	Servicebio	G3330-100
SDS-PAGE gel kit	JingCai	JC-PE022/R
BCA protein quantification kit	BiYunTian	P0012
TUNEL Apoptosis Kit	Servicebio	G1504
Dual luciferase activity detection kit	ZeYe Biotech	ZY130595
riboFECTTM CP Reagent	RuiBo	C10511-05
Experimental models: Cell lines		
SKOV3/DDP	ChuanQiu Biotech	A016
A2780/DDP	ChuanQiu Biotech	A001
SKOV3	ChuanQiu Biotech	CL-0215
A2780	FuHeng Biology	FH-0140
IOSE-80	WanWu Biology	tings-1618133
Experimental models: Organisms/strains		
BALB/c nude mice	Beijing Sibeifu	N/A
Oligonucleotides		
S100A4 Forward (5′-3′): CAGAACTAA AGGAGCTGCTGACC	This paper	N/A

(*Continued on next page*)

Continued

REAGENT or RESOURCE	SOURCE	IDENTIFIER
S100A4 Reverse (5′-3′): CTTGGAAG TCCACCTCG -TTGTC	This paper	N/A
GAPDH Forward (5′-3′): GTCTCCTCT GACTTCAACAGCG	This paper	N/A
GAPDH Reverse (5′-3′): ACCACCCTGTTGCTGTAGCCAA	This paper	N/A
siRNA oligonucleotides targeting S100A4 : 5′-UCCAGAAGCU- GAUGAGCAATT-3′	QingKe Biology	N/A
siRNA oligonucleotides targeting control: shUUCUCCGAACGUGUCACGUTT	QingKe Biology	N/A
Recombinant DNA		
PCDNA3.1 + S100A4	QingKe Biology	N/A
PCDNA3.1 + NF-κB p65	QingKe Biology	N/A
Software and algorithms		
GraphPad Prism 8	GraphPad	N/A
Other		
DDP	Solarbio	IC0440
McCoy's 5A	Procell	PM150710
DMEM	Solarbio	12100-500
FBS	BIOIND	04001-1ACS

RESOURCE AVAILABILITY

Lead contact

Further information and requests for resources and reagents should be directed to and will be fulfilled by the lead contact, Ming Gao (gaoming330949@126.com).

Materials availability

This study did not generate new unique reagents. All the cell lines used in this manuscript will be made available upon request. A material transfer agreement will be required prior to sharing of materials.

Data and code availability

Data reported in this paper will be shared by the lead contact upon request. This paper does not report original code.

Any additional information required to reanalyze the data reported in this paper will be made available by the lead contact upon request.

EXPERIMENTAL MODEL AND STUDY PARTICIPANT DETAILS

Ethics approval and consent to participate

The study was approved by the Medical Ethics Committee of the First Affiliated Hospital of Zhengzhou University (certificate number 2023-KY-0866-001). The care and use of these experimental animals was in accordance with institutional guidelines. All the authors consented to participate in this study.

Cell lines

Two ovarian cancer cell lines exhibiting cisplatin resistance, denoted as SKOV3/DDP and A2780/DDP, were sourced from Shanghai Chuanqiu Biotechnology Co., Ltd. Cisplatin (DDP, IC0440) was obtained from Beijing Solarbio Science and Technology Co., Ltd. IOSE-80 cell line was acquired from Hefei Everything Technology Co., Ltd. (Anhui, China), A2780 cell line was acquired from FuHeng Biology, SKOV3 cell line was acquired from Shanghai Chuanqiu Biotechnology Co., Ltd. Cells were cultured in McCoy's 5A (Cat. PM150710, Procell) or DMEM (Cat. 12100-500, Solarbio), added with 1% Penicillin-Streptomycin, 10% fetal bovine serum (Cat. 04001-1ACS, BIOIND) at 37°C with 5% CO_2.

Mice

Five-week-old female nude mice (BALB/c nude mice, Spiff, Beijing, China) were procured for the experiment and housed in a temperature- and humidity-controlled environment on a 12-h light/dark cycle.

METHOD DETAILS

Transfection

For transfection, cells were cultured to achieve a density of 70%-80%. Subsequently, the culture medium was replaced with fresh medium, and the cells were incubated at 37°C. The plasmid storage solution was diluted with 1X riboFECT CP Buffer (Cat. C10511-05, RuiBo) in an EP tube, followed by thorough mixing and incubation at room temperature for 5 min. The riboFECT CP Reagent was then added, gently mixed, and allowed to incubate at room temperature for 15 min. The riboFECT CP mixture was introduced into the cell medium and gently mixed. The culture plate was subsequently placed in a CO_2 incubator at 37°C for a duration of 24–96 h. The efficiency of transfection was assessed 24–72 h post-transfection via western blot analysis. siRNA oligonucleotides targeting S100A4 (target sequence: 5′-UCCAGAAGCUGAUGAGCAATT-3′) and silencer-negative siRNA for control were procured from Qingke Biology Co., Ltd.

CCK8 testing

During the logarithmic growth phase, routine digestion and centrifugation were performed, and the cells were adjusted to a density of 1×10^4 cells per well, followed by inoculation into a 96-well culture plate. Each well was supplemented with 100 μL of DMEM, and a concentration gradient was established. Specifically, the EGCG group comprised concentrations of 0 (blank group), 10, 20, 30, and 40 μmol/L. Following cell adhesion, different concentrations of EGCG and DDP were added to the wells. After 72 h of routine culture, 100 μL of CCK-8 reagent (Cat. C200-100, OuSe Biotech) was introduced to each well, and the absorbance at 450 nm was measured via enzyme labeling following a 2-hour incubation period. The inhibition rate of the control group was determined to be 0%.

RNA extraction, reverse transcription and real-time quantitative PCR

Total RNA was extracted employing TRIzol reagent (Cat. 15596026, Invitrogen). Subsequently, 0.1–0.5 μg of RNA was introduced into a sterile enzyme-free PCR tube. To this solution, 1 μL of Oligo (dT)18 Primer (50 μm), 4 μL of 5× Reaction Buffer, 1 μL of Servicebio®RT Enzyme Mix, and enzyme-free sterile water were supplemented to a final volume of 20 μL. PCR was conducted at 25°C for 5 min, followed by 42°C for 30 min, and finally 85°C for 5 s to yield cDNA.

The reaction system was configured as follows: 10 μL of 2× SYBR Green qPCR Master Mix (Cat. G3321-15, Servicebio), 0.4 μL of Forward Primer, 0.4 μL of Reverse Primer, and 1.0 μL of cDNA. An Agilent Mx3000P real-time fluorescence quantitative PCR instrument was employed for PCR. The amplification procedure consisted of an initial denaturation step at 95°C for 10 min, followed by 40 cycles of denaturation at 95°C for 15 s, annealing at 62°C for 30 s, and extension at 72°C for 30 s, with a final melting curve from 60°C to 95°C, increasing in temperature by 0.5°C every 15 s. Each sample was subjected to at least 3 replicates. Amplification curves were obtained and subjected to data analysis. The relative expression level of the samples was calculated, and statistical analysis was performed.

Western blot analysis

Total proteins were extracted through cell lysis using protease inhibitors and RIPA lysis buffer (Cat. JC-PL001, JingCai) (comprising 50 mM Tris (pH 7.4), 150 mM NaCl, 1% Triton X-100, 1% sodium deoxycholate, 0.1% SDS, EDTA, and similar constituents). Protein concentration detection was conducted using BCA buffer. Protein denaturation was achieved with 5× reduced protein loading buffer. Subsequently, proteins were separated via SDS-PAGE (Cat. JC-PE022/R, JingCai), transferred onto PVDF membranes, and probed with primary antibodies. Immunoreactive material was visualized employing an ECL method.

Immunohistochemical (IHC) staining

The experimental procedure was conducted on serial paraffin-embedded sections of 3–5 μm thickness. Initially, the sections were heated at 70°C for 30 min. The dewaxing and rehydration processes involved sequential treatments: xylene I for 20 min, xylene II for 20 min, anhydrous ethanol for 5 min, 75% ethanol for 5 min, and distilled water for 5 min. Antigen retrieval was performed by microwaving the sections in EDTA (Cat. BL727B, iosharp) solution at medium heat for 8 min, followed by a 7 min interval without heating, then medium-low heat for 7 min, and subsequently cooling to room temperature. For blocking, BSA was applied for a duration of 50 min.

The sections were incubated overnight at 4°C with primary antibodies, followed by incubation with secondary antibodies. DAB (Cat. G1212-200T, servicebio) and hematoxylin staining were carried out, and subsequently, the sections were subjected to dehydration and clearing. A drop of neutral gum was used for mounting the cover glass.

TUNEL apoptosis assay

Adherent cells were cultured in 24-well plates. After induction of apoptosis, slides were gently washed with PBS. Fixation was achieved by adding 4% paraformaldehyde solution to each well, followed by incubation at room temperature for 20 min, and then washed with PBS three times. Permeabilization was carried out with a suitable volume of permeable liquid at room temperature for 20 min, and the permeable liquid was subsequently removed. Then, 50 μL of equilibration buffer was added to each sample to cover all sample areas, and the samples were incubated at room temperature for 20 min. A mixture of CF640-dUTP Labeling Mix and Equilibration Buffer was prepared, and for positive reactions, recombinant TDT enzyme: CF640-DUTP Labeling Mix: Equilibration Buffer = 1 μL:5 μL: 50 μL was used. A control TdT incubation buffer devoid of recombinant TdT enzyme was prepared and replaced with ddH_2O for the negative control system. Excess equilibration buffer was removed, and then 56 μL of TdT incubation buffer was added to each tissue sample, taking care not to let the slides dry to avoid

exposure to light. The slides were placed in a humid box and incubated at 37°C for 2 h, followed by washing the tissue samples with PBS four times. DAPI solution (2 μg/mL) was added in the dark, and after rinsing with PBS, the samples were immediately examined using a fluorescence microscope.

Transwell invasion test

In the upper chamber of the Transwell apparatus, 50 μL of Matrigel matrix gel (Matrigel diluted with serum-free and anti-antibody medium at a 1:8 ratio) was applied, and the upper medium was desiccated in an incubator at 37°C for 5 h. Following solidification of the Matrigel matrix, the upper medium was evacuated. Cells, at a density of 1×10^5 cells/mL, were gathered and introduced into the upper chamber of the Transwell unit. The culture medium supplemented with EGCG was added, while DMSO served as the control. Additionally, 500 μL of medium containing 20% FBS was added to the lower chamber. The cells were then incubated in a 37°C incubator with 5% CO_2 for a duration of 24 h. Subsequently, the cells on the inner chamber membrane were eliminated using cotton swabs, fixed in 4% paraformaldehyde for 15 min, dried, and stained with crystal violet for 20 min. Following staining, the samples were washed with ultrapure water. Once dried, the chamber was inverted under the microscope, and the average cell count was computed for comparison.

Wound healing test

Cells at the logarithmic growth phase were categorized into a blank control group, an EGCG group (20 μmol/L), and pancreatic protein cells. After enzymatic digestion, the cells were inoculated into 6-well plates, and the plate backs were marked accordingly. When cell growth density reached approximately 80% to 90%, a straight line was drawn into the wells using a 100 μL pipette tip, ensuring uniform pressure. After three washes with PBS, serum-free DMEM was added. The plates were then placed in a 37°C incubator with 5% CO_2, and photographs were captured after 24 and 48 h of culture.

Colony formation

A cell suspension was diluted to a gradient, and 200 cells were inoculated into each experimental group in a 6-well culture plate, ensuring even cell dispersion. The cells were cultured at 37°C with 5% CO_2 for a duration of 2 weeks. The culture medium was replaced every 3 days until the vast majority of single colonies contained more than 50 cells. Subsequently, 4% paraformaldehyde (5 mL) was used to fix the cells for 15 min. Following fixation, an appropriate volume of Giemsa stain was added, and the staining solution was applied for 20 min. A transparent film with a grid was overlaid on the plate, and the number of colonies, or colonies consisting of more than 10 cells, was counted under a microscope (low-power lens). Finally, the colony formation rate was calculated as follows: Colony formation rate = (number of colonies/number of inoculated cells) ×100%.

Double luciferase experiment

The medium was aspirated from the cell well to be tested, followed by rinsing the cells thrice with 1× PBS, after which the PBS was removed. Subsequently, 100 μl of 1× PLB lysis buffer was added to each well. The 24-well plate was then agitated for 20-30 minutes. The Promega equipment was reset for testing and programmed for dual luciferase detection. For the assay, 50 μL of LAR II and 10 μL of cell lysate were combined in a 1.5 ml EP tube, mixed thrice, and then placed in the detector for initial. After the measurement, the EP tube was removed, 50 μL of Stop & Glos Reagent was added, mixed, and the tube was placed back in the detector for a second reading. All readings, the process, and the analysis of the experimental results were meticulously recorded.

Nude mice tumorigenicity assay

Each mouse received a subcutaneous injection of 200 μL of normal saline containing A2780/DDP cells (cell concentration 1×10^6/mL) on the right side. After 7 days of injection, the mice were randomly allocated into 2 groups (n = 5/group): the blank group and the EGCG group. In the blank group, intraperitoneal injection of normal saline was administered, while the EGCG group received intraperitoneal injections of 50 mg/kg EGCG every three days. Tumor volume was calculated using the formula: Volume = length × $\text{width}^2/2$. The volume of each mouse was measured weekly.

QUANTIFICATION AND STATISTICAL ANALYSIS

The comparisons between two groups were assessed by Student's t tests, and the statistical differences among groups were determined by one-way ANOVA followed by Tukey-Sidak's multiple comparison. Figures depict values as the mean ± SD. P-values less than 0.05, 0.01, and 0.001 were considered statistically significant. Statistical calculations were performed using GraphPad Prism 8 (San Diego, CA, USA).